OXFORD

Cerebral Cortex, December 2020;30: 6238–6253

doi: 10.1093/cercor/bhaa181
Advance Access Publication Date: 13 July 2020
Original Article

ORIGINAL ARTICLE

Disruption and Compensation of Sulcation-based Covariance Networks in Neonatal Brain Growth after Perinatal Injury

Sharon Y. Kim[1,†], Mengting Liu[1,†], Seok-Jun Hong[2], Arthur W. Toga[1], A. James Barkovich[3], Duan Xu[3] and Hosung Kim[1]

[1]Laboratory of Neuro Imaging at USC Stevens Neuroimaging and Informatics Institute, Keck School of Medicine of USC, University of Southern California, 2025 Zonal Ave, Los Angeles, CA 90033, USA, [2]Center for the Developing Brain, Child Mind Institute, New York, NY 10022, USA and [3]Department of Radiology, School of Medicine, University of California San Francisco, 1 Irving St., San Francisco, CA 94143, USA

Address correspondence to Mengting Liu Laboratory of Neuro Imaging at USC Stevens Neuroimaging and Informatics Institute, Keck School of Medicine of USC, University of Southern California, 2025 Zonal Ave, Los Angeles, CA 90033, USA. Email: mliu@ini.usc.edu.

[†]These authors contributed equally to the study

Abstract

Perinatal brain injuries in preterm neonates are associated with alterations in structural neurodevelopment, leading to impaired cognition, motor coordination, and behavior. However, it remains unknown how such injuries affect postnatal cortical folding and structural covariance networks, which indicate functional parcellation and reciprocal brain connectivity. Studying 229 magnetic resonance scans from 158 preterm neonates ($n = 158$, mean age = 28.2), we found that severe injuries including intraventricular hemorrhage, periventricular leukomalacia, and ventriculomegaly lead to significantly reduced cortical folding and increased covariance (hyper-covariance) in only the early (<31 weeks) but not middle (31–35 weeks) or late stage (>35 weeks) of the third trimester. The aberrant hyper-covariance may drive acceleration of cortical folding as a compensatory mechanism to "catch-up" with normal development. By 40 weeks, preterm neonates with/without severe brain injuries exhibited no difference in cortical folding and covariance compared with healthy term neonates. However, graph theory-based analysis showed that even after recovery, severely injured brains exhibit a more segregated, less integrated, and overall inefficient network system with reduced integration strength in the dorsal attention, frontoparietal, limbic, and visual network systems. Ultimately, severe perinatal injuries cause network-level deviations that persist until the late stage of the third trimester and may contribute to neurofunctional impairment.

Key words: cortical folding, covariance networks, graph theory, perinatal brain injury, prematurity

Introduction

Preterm infants are at profound risk for neurological deficits across several domains, including cognition, motor coordination, and behavior (Woodward et al. 2006; Geva et al. 2014). Such deficits are usually not detected until later childhood, and it is often difficult to pinpoint the developmental origin and mechanism for impairment (Kodric et al. 2014; Maggi et al. 2014). Various perinatal brain injuries, such as intraventricular hemorrhage (IVH), white matter injury (WMI), including focal cystic necrotic lesions (commonly called periventricular leukomalacia or PVL) and noncystic white matter abnormalities (Miller et al. 2003) as well as ventriculomegaly (VM) are leading

drivers of neurodevelopmental deficits (Hamrick et al. 2004; Miller et al. 2005) (Table 3). Despite the abundance of studies that have attempted to characterize normative patterns of early brain growth, little is known regarding the influence of perinatal brain injury on early structural development coursing from prenatal to postnatal childhood. Thus, it remains a paramount goal to identify how specifically perinatal neurological injuries affect the developmental trajectory of cerebral morphology and network connectivity in the early postnatal time frame.

Among various morphological characteristics, cortical folding is indicative of early development of the brain as a connected system. For instance, it has been hypothesized that cortical folding is driven by multiple factors (Ronan and Fletcher 2015) including 1) tangential expansion of the cortex causing an increase in tangential pressure or tension along white matter axons in cortico-cortical connections (Van Essen 1997; Chen et al. 2013; Zilles et al. 2013) and 2) proliferative radial glial cell units originating from the cerebral ventricle that evolve into a mosaic of interrelated ontogenetic columns responsible for cerebral morphological development (Rakic 1988). Furthermore, cortical folding is an established biomarker of brain functional development (Dubois et al. 2008) and is dependent upon a highly coordinated neural proliferative process of radial glial cells that dictate cortical folding and parcellate the cerebrum into cytoarchitectonic areas (Rakic 1988). And in contrast to other cortical morphology, cortical folding uniquely expands dramatically within the third trimester during which most secondary sulci and gyri have formed (Chi et al. 1977; White et al. 2010)

The dramatic expansion of cortical folding primarily occurring in the 3rd trimester is also the period when most preterm births occur, making it crucial to examine the brain in this specific window of neurodevelopment. Not surprisingly, abnormal cortical folding is associated with numerous neuropsychiatric and developmental disorders (Van Essen et al. 2006; Nordahl et al. 2007; Cachia et al. 2008). Past studies importantly demonstrate that preterm birth and its associated injuries lead to aberrant cortical folding (Lefevre et al. 2016). Likewise, analysis of cortical folding in nonhuman primates demonstrated that neurological insult interestingly drives the onset of new and aberrant cortical folding at specific periods of gestation (Goldman-Rakic and Rakic 1984). However, no study to date has elucidated how neurological injury affects folding expansion and its associated covariance networks specifically in preterm neonates.

In order to measure cortical folding patterns, our study leveraged the sulcal depth metric variation along regional sulcation and gyration. This sulcal depth measurement is a 3D form of quantifying cortical folding complexity, extending upon the seminal 2D gyrification index (Zilles et al. 1988). We deemed sulcal depth as the superior parameter for covariance analysis, since sulcal depth has the highest density and overlap of corticocortical connections as well as weak thalamic projections (Goldman-Rakic and Schwartz 1982) as opposed to gyri which receive strong projections from the thalamus (Welker and Campos 1963). In fact, innervation to the cortex by brain stem monoamine input is more abundant in the sulcal invaginations than at the curvature of gyri (Levitt et al. 1984).

However, although quantitative analysis of cortical folding may uncover pathological deviations, it alone may not have the capacity to fully elucidate the structural or functional integration and segregation among different brain regions. Structural covariance networks are derived from statistically robust correlations between morphometrics measured in two brain regions and are highly coordinated throughout maturational events from the embryo through adulthood (Mechelli et al. 2005; Lerch et al. 2006). They are observed in normally developing and aging brains (Raznahan et al. 2011; Khundrakpam et al. 2013) and are altered in numerous diseases including Alzheimer's Disease, schizophrenia, multiple sclerosis, and autism (Bassett and Bullmore 2009; Sharda et al. 2016). Although altered structural covariance is known to be present in adolescents who survived after preterm birth (Nosarti et al. 2011), it is unknown whether such alterations are a result of perinatal brain injuries or postnatal changes.

The purpose of our study, using a large database of preterm neonates, was to compare 1) cortical folding measurements, 2) sulcation-based structural covariance networks, and 3) Bayley Scales of Infant Development measured at age 18 months among three groups: healthy term (HT); noninjured to mildly injured (NMI) preterm; and severely injured (SI) preterm neonates (defined in the Methods). We partitioned the third trimester (26–40 weeks of GA) into equidistant three-time frames (early: 26–30 weeks, middle: 31–35, late: 36–40) to capture spatiotemporal patterns of each group's cortical folding and covariance networks in the 3rd trimester—a developmental period critical for the folding process. We hypothesized that, compared with NMI preterm neonates and term neonates, SI preterm neonates would exhibit a temporally varying pattern of pronounced aberration in the regional morphology and covariance/coupling of cortical folding. Our study is the first to spearhead novel structural covariance analysis of cortical folding in term and preterm neonates.

Materials and Methods

Subjects

Our dataset comprised of 158 preterm (mean postmenstrual age at birth [PMA] = 28.3 ± 1.9 weeks; range 24–33 weeks), admitted to UCSF Benioff Children's Hospital San Francisco between June 2006 and March 2015 (Table 1). Most subjects were scanned twice but some scans were excluded due to a large amount of motion artifact, resulting in a total of 229 MRI scans. Other exclusion criteria included 1) clinical evidence of a congenital malformation or syndrome, 2) congenital infection, and 3) newborns too clinically unstable for transport to and from the MRI scanner. Parental consent was obtained for all cases following a protocol approved by the Institutional Committee on Human Research. All patients were scanned postnatally as soon as they were clinically stable (PMA at scan: 31.6 ± 1.8 weeks; range 26.7–43 weeks), and 71 patients were rescanned before discharge at late preterm age. Sedation was used only with parental consent and when subjects initially moved enough to cause imaging artifact. Approximately 50% of the cohort received sedation, usually pentobarbital in small doses. In the current study, we also included 40 term newborns scanned through the Developing Human Connectome Project (dHCP, http://www.developingconnectome.org) for the comparison of healthy development with the standardization of preterm neonate's features.

MRI Acquisition

Customized MRI-compatible incubators with specialized head coils were used to provide a quiet, well-monitored environment

Table 1 Demographic and clinical characteristics for preterm neonates

Demographic	
Subjects (*n*)	158
MRI scans (*n*)	229
Sex: male (*n*)	131
GA at birth (weeks, mean ± SD)	28.2 ± 2.0
PMA at MRI	
1st scans	31.6 ± 1.9
2nd scans	35.9 ± 1.9
Characteristic [a]	**Number (%)**
Maternal/antenatal factors	
Maternal age, years	30.0 ± 7.2
Placenta previa	9 (10.2)
Drug abuse[b]	5 (5.7)
Magnesium sulfate	62 (70.5)
Exposure to prenatal steroids	80 (90.9)
Chorioamnionitis	18 (20.5)
Delivery/perinatal factors	
Twin	35 (39.8)
Birth weight, g	1081 ± 326.8
Caesarean section delivery	55 (62.5)
Postnatal factors	
Exposure to postnatal steroids	11 (12.5)
Hypotension	48 (54.5)
Infant infection	56 (63.6)
Patent ductus arteriosus	45 (5.11)
Necrotizing enterocolitis[c]	4 (4.5)
Duration of intubation, days	9.9 ± 21.0
Chronic lung disease	21 (23.9)

Note: Numbers and percentages were derived from 88 preterm subjects whose data was recorded and known.
[a]Data presented as number (%) or mean ± standard deviation.
[b]All subjects with maternal smoking (based on self-report) were exposed to marijuana, two were also exposed to tobacco.
[c]It was diagnosed based on Bell's stage II criteria (Kliegman et al. 1982).

for neonates during the MRI scan, minimizing patient movement and improving the signal-to-noise ratio. Newborns enrolled between June 2006 and July 2011 ($n = 156$) were scanned on a 1.5-Tesla General Electric Signa HDxt system (GE Medical Systems) using a specialized high-sensitivity, receive-only quadrature birdcage neonatal head coil built within a custom-built MRI-compatible incubator (Dumoulin et al. 2002). T1-weighted images were acquired using sagittal 3-dimensional inversion recovery spoiled gradient echo (3D IR SPGR) (repetition time [TR] = 35; echo time [TE] = 6.00; inversion time of 0.00 ms; field of view [FOV] = 256 × 192 mm^2; number of excitations [NEX] = 1.00; and flip angle [FA] = 35°), yielding images with 1 × 1 × 1 mm^3 spatial resolution. The in-plane resolution for the 1.5 T is 1 mm × 1 mm and 3 mm thick. Newborns enrolled between July 2011 and March 2015 ($n = 73$) were scanned on a 3-Tesla General Electric Discovery MR750 system in a different MR compatible incubator and using a specially designed (for 3 T imaging) neonatal head coil. T1-weighted images were also acquired using sagittal 3D IR-SPGR (TR = minimum; TE = minimum; inversion time of 450 ms; FOV = 180 × 180 mm^2; NEX = 1.00; FA = 15°), and were reformatted in the axial and coronal planes, yielding images with 0.7 × 0.7 × 1 mm^3 spatial resolution. The in-plane resolution for the 3 T is 1 mm × 1 mm and 2 mm thick.

T2-weighted images were acquired to examine for areas of encephalomalacia or malformations using the parameters TR = 5000 ms; TE = 120 ms; FOV = 200 mm; NEX = 2.0; slice thickness = 3 mm. Susceptibility-weighted images (SWI) were acquired to examine for hemorrhages and calcifications with the parameters TR = 46 ms; TE = 28 ms; FA = 20°; FOV = 180 mm; NEX = 1.0; slice thickness = 2.0 mm. The scan times for T1w, T2w and SWI were approximately 3.5, 2.5 and 5 min, respectively.

For 40 dHCP controls, we analyzed T1 images which were acquired using an IR TSE sequence with the resolution of 0.5 × 0.5 × 0.5 mm^3 with TR = 4.8 s, TE = 8.7 ms.

Diagnosis of Neonatal Brain Injuries

A pediatric neuroradiologist (A.J.B.) blinded to patient history reviewed patient MRI scans including 3-D T1 and axial T2-weighted sequences, as well as SWI when available. Presence and severity of IVH, hydrocephalus (i.e., VM), and WMI were evaluated (Table 2). The spectrum of WMI includes focal cystic necrotic lesions (periventricular leukomalacia; PVL) and noncystic lesions. The severity scores were generated for IVH using the scoring system of Papile (0: absent; 1: germinal matrix hemorrhage; 2: IVH; 3: IVH with hydrocephalus; 4: parenchymal hemorrhage, usually periventricular hemorrhagic infarction) (Papile et al. 1978) and WMI (0: absent; 1: <3 foci, <2 mm; 2: ≥3 foci, >2 mm; 3: >5% hemisphere) using established criteria (Papile et al. 1978; Miller et al. 2003). Subsequently, IVH scores were binarized with "mild" representing grades 1–2, and "severe" representing grades 3–4; WMI and VM were categorized as "mild" for grade 1 and "severe" for grades 2–3. For subjects with multiple MR examinations, the highest (most severe) score in each category was used for analysis. In the current study, we compared cortical folding patterning and covariance networks between the none-mild injury group and severe injury group. We merged infants with mild injuries and those with no injury into one none-mild injury group, since the two groups exhibited no significant differences in the following analyses.

Measurement of Sulcus Depth to Characterize Sulcation

T1-weighted MRI scans were used to obtain sulcal depth measures using the NEOCIVET pipeline (Kim, Lepage, et al. 2016b) developed based on CIVET at the Montreal Neurological Institute (http://www.bic.mni.mcgill.ca/ServicesSoftware/CIVET). The steps involved are given as follows: First, the native MRI images were corrected for nonuniformity artifacts using N3 algorithm and registered into the stereotaxic space using a linear transformation. Different types of brain tissue (GM, WM, and CSF) were segmented with an advanced label fusion based on a joint probability between selected templates. Next, WM surface was automatically extracted by evolving an ellipsoid, triangulated using an icosahedral model and a multiresolution deformation scheme; Then the cortical morphology was characterized by measuring sulcal depth within the two surfaces at 81 924 vertices (163 840 polygons) throughout the cortex. Finally, sulcal depth was further resampled to the age-specific surface template (Kim, Lepage, et al. 2016b) using the transformation obtained in the surface registration, in order to allow intersubject comparison.

Construction of Corticocortical Covariance Network

All neonates were divided into three groups based upon their age ranges and the uniform subdivision (early: <31 weeks;

Table 2 Definition and categorization of neurological injuries

Factor	Category (n = scans)	
	None-mild injury	Severe injury
IVH (Ahmann et al. 1980; Volpe 1981) - Bleeding into the ventricles of the brain. - Overall occurrence rate of approximately 15%. - IVH occurs in 40% of premature neonates who weigh less than 1500 g.	Grade 0–2 (n = 159)	Grade 3–4 (n = 56 scans)
VM (Perlman and Rollins 2000; Mehlhorn et al. 2017) -Dilatation of the lateral cerebral ventricles, usually defined as greater than 10 mm at the level of the atria. -Prevalence of 0.3–1.5 per 1000 live births.	Grade 0–1 (n = 208)	Grade 2–4 (n = 33)
WMI (Perlman et al. 1996; Volpe 1997; Imamura et al. 2013) -Type of brain damage that affects the brain's white matter and can lead to a series of disabilities, including cerebral palsy. -Reported incidence of PVL varies from 3% to 15%. -Periventricular leukomalacia is seen in 3% to 10% of premature neonates.	Grade 0–1 (n = 196)	Grade 2–3 (n = 57)

Table 3 MRI scan categorization

	Early <31 weeks n = 57		Middle 31–35 weeks n = 99		Late >35 weeks n = 73		Healthy term ~40 weeks n = 40
	None—mild injury	Severe injury	None—mild injury	Severe injury	None—mild injury	Severe injury	Healthy
Subjects (n)	n = 42	n = 15	n = 79	n = 20	n = 50	n = 23	n = 40
Males	36	14	64	18	42	19	25:15
Birth age ± SD (range)	27.6 ± 1.5 (5.6)	26.8 ± 1.6 (4.6)	28.8 ± 1.7 (6.7)	28.9 ± 2.3 (8.3)	28.6 ± 2.0 (7.3)	28.1 ± 2.1 (6.9)	39.0 ± 1.7 (5.6)
Scan age ± SD (range)	29.9 ± 0.8 (3.7)	29.9 ± 1.1 (4.2)	32.7 ± 1.1 (3.8)	33.1 ± 1.2 (3.7)	36.4 ± 1.3 (5.3)	36.5 ± 1.3 (5.0)	39.9 ± 2.1 (7.3)
Birth weight (g)	982	964	1158	1188	1110	1129	Not available

middle: 31–35 weeks; late 3rd trimester: >35 weeks) and each group was subgrouped again into either none-mild or severe injury groups based on injury severity grades listed in Tables 2 and 3.

A general linear model (GLM) was used to account for covariance between vertices while accounting for confounding variables including PMA at birth, sex, and MRI field strength (3 T vs. 1.5 T). Next, correlation matrices of sulcal depth showing anatomical coupling among cortical regions at whole brain level were computed for each group (Lerch et al. 2006; Raznahan et al. 2011). As a correlation matrix computed across all 81 924 vertices requires extremely expensive computational times, all vertices across the whole cortex were further evenly sampled to 1284 vertices on which correlation maps were constructed, while avoiding any bias associated with anatomical parcellation (Fig. 1).

Network Analysis

For graph-theoretic analysis, correlation matrices were first binarized based on sparsity thresholding. We defined sparsity as the total number of edges in a graph divided by the maximum possible number of edges. The binarized graphs were used to calculate global efficiency and shortest characterized path length, clustering coefficient, and modularity. The details of each index are described below.

Properties of Covariance Networks

The patterns of relationship among brain regions within a network can be described using two distinctive topological properties: segregation and integration (Rubinov and Sporns 2010).

For graph-theoretic analysis, the correlation matrices were first binarized based on sparsity thresholding. We defined sparsity as the total number of edges in a graph divided by the maximum possible number of edges. Fixing a sparsity threshold (for instance, x% threshold denotes x% of the topmost connections) assured the same number of edges for graphs of different groups. In order to determine proper assessment of network properties and nominal spurious number of edges in each network, we used a range of sparsity threshold $2 \leq S \leq 40$, increased with a step of 2. A sparsity threshold of 10 is used in main text and results with all other sparsity threshold can be found in Supplementary Information (Supplementary Figs 1–3).

Binarized graphs were used to calculate measures of 1) network integration: global efficiency and shortest characterized path length and 2) network segregation: clustering coefficient and modularity. Details of each network index are described below.

Network Integration

The *characteristic path length* L of a network was defined as the mean minimum number of edges between any two nodes, that

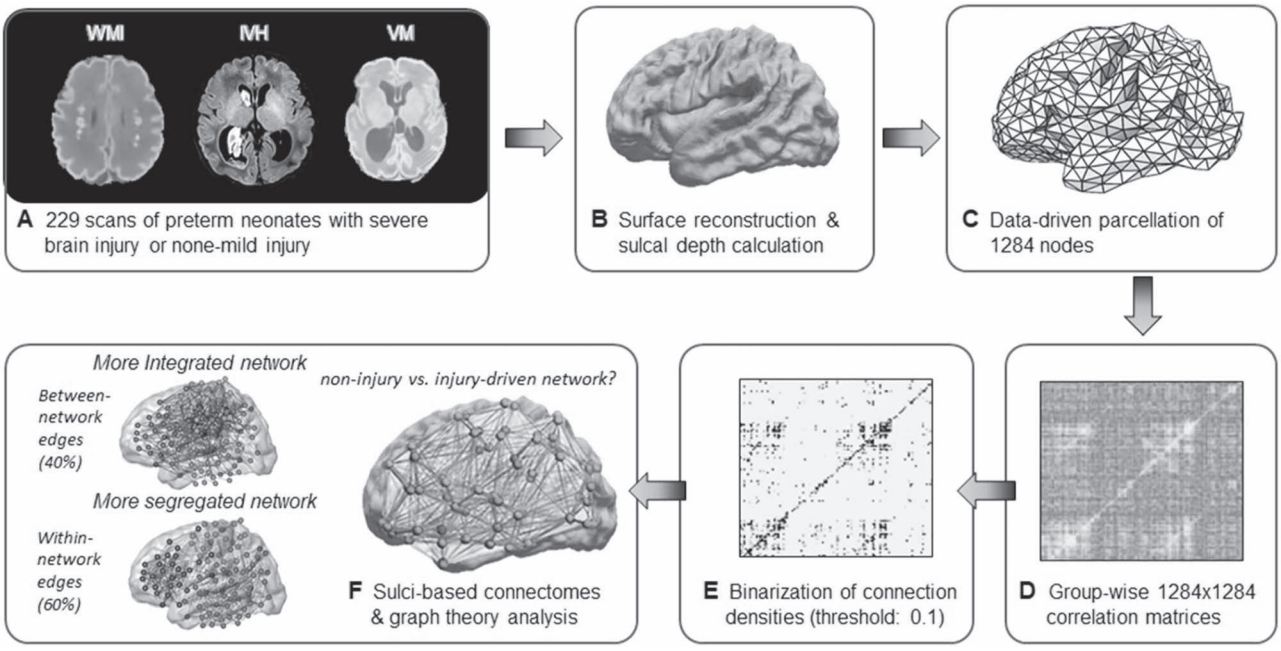

Figure 1. Overview of processing sulcation-based covariance networks. (*A*) MR scans of preterm neonates were separated into two groups: subjects with none-mild brain injury and those with severe brain injury (order: WMI, IVH, VM). (*B*) Using MR scans, sulcal depth values were extracted after surface reconstruction using the pipeline NEOCIVET. (*C*) 81 924 vertices of sulcal depth values were evenly subsampled into 1284 vertices. (*D*) Correlation matrices were derived by calculating correlations between regional sulcation across subjects within each group separately. (*E*) Binarized adjacency matrices were derived from the correlation matrices using a range of sparsity threshold $2 \leq S \leq 40$ (i.e., top 2–40% of strongest connections for fully connected graphs in both groups). (*F*) Sulci-based connectomes were then analyzed using graph theory metrics of segregation and integration.

is, the shortest path $L_{i,j}$. $L_{i,j}$ between nodes i and j is defined as the lowest number of edges that must be traversed to go from i to j. A node's average path length $L(i, G)$ is the average length of the shortest paths between i and all other nodes. Accordingly, the global efficiency, E, of a graph G is as follows:

$$E(G) = \frac{1}{N(N-1)} \sum_{i \neq j \in G} \frac{1}{L_{i,j}}$$

Global efficiency can be interpreted as the capacity for integrative information transfer across the network (Rubinov and Sporns 2010).

Network Segregation

We computed the *clustering coefficient* using standard formulas (Watts and Strogatz 1998). These quantities are widely used graph-theoretical parameters to describe network topology. *Clustering coefficient* C_i of a given node i was defined as

$$C_i = \frac{T_i}{k_i(k_i - 1)/2}$$

Where T_i is the number of existing connections among the neighbors of node i. As k_i is the actual number of neighbors of node i (i.e., its degree), the denominator term $k_i \times (k_i - 1)/2$ quantifies the number of all possible connections among the neighboring nodes. If a node i had only one edge or no edges, C_i was set to 0. Mean network clustering C was defined as the average of C_i over all nodes.

Modularity is a measure of the degree to which a graph is organized into distinct subgraphs (Rubinov and Sporns 2010). The *modularity* algorithm attempts to partition the graph into disjoint subgraphs, in such a way as to minimize the degree of intermodule connectivity and maximize intramodule connectivity. This ratio is captured in the parameter Q. The modularity, Q, of a graph G is a function of the proportion of G's edges that fall within modules (topological communities of varying size). This can be defined as follows:

$$Q(G) = \frac{1}{2m} \sum_{i \neq j} \left(A_{i,j} - p_{i,j}\right) \delta\left(M_i, M_j\right)$$

where m is the total number of edges; $A_{i,j} = 1$ if an edge links i and j and 0 otherwise; $\delta(M_i, M_j) = 1$ if i and j are in the same module and 0 otherwise; and $p_{i,j}$ is the probability that a random graph with the same degree distribution as G has an edge between i and j, as follows:

$$p_{i,j} = \frac{k_i k_j}{2m}$$

Where k_i is node i's degree. Nodes should be assigned to modules to yield the largest possible Q, which is approximated using a simulated annealing algorithm. For the analysis of community structure, nodes were assigned to their most stable modules based on 10 runs of the simulated annealing algorithm.

The graph theory metrics that are analyzed in the current study are summarized in Supplementary Table 5.

Analysis of Large-Scale Networks

As a measure of connectivity, the correlation strength for each pair of vertices and for each of group of infants was computed separately. The correlation strength was then Fisher

z-transformed. No threshold was applied to the correlation coefficients, that is, resulting networks were weighted and signed.

For subnetwork construction, we used the Automated Anatomical Labeling (AAL) parcellation of the cortex and subcortical regions which consist of 90 Region-of-Interests (ROI). For each of the subnetwork, a set of network ROIs that have been demonstrated to be representative for the networks under investigation (Power et al. 2011) were utilized. All vertices within each ROI were assigned to any of nine well-established large-scale networks, comprising low-level input and output networks (visual, auditory and sensorimotor networks), subcortical nodes, the default mode network (DMN), ventral and dorsal attention networks, cognitive control networks including frontoparietal network and limbic network, and salience network.

Mean connectivity between and within networks was computed as the average across all edges between/within those networks. To quantify the degree of integration and segregation for global brain network, we then introduce the network metric Segregation Integration Difference (SID) that operates on correlation strength at the level of subnetworks. For example, if we assume that the whole brain network is divided into a total of M subnetworks, we define global SID subnetworks as

$$\mathrm{SID} = \sum_{m=1}^{M}\sum_{n=1}^{M}\left(\frac{2}{N_m\,(N_m-1)}\sum_{i,j\in m}A_{i,j} - \frac{1}{N_m N_n}\sum_{p\in m,q\in n}A_{p,q}\right)$$

Where $A_{i,j}$ is the correlation strength within subnetwork m, and $A_{p,q}$ is the correlation strength between subnetworks m and n. N_m and N_n are the number of vertices within the m and n subnetworks, respectively.

Accordingly, it is possible to extend the scope of the SID measure so that we can compute an estimate of integration-segregation degree for specific network. If we assume that the whole brain network is divided into a total of M subnetworks, the SID parameter for subnetwork m with respect to all other subnetworks is defined as

$$\mathrm{SID}_m = \sum_{n=1}^{M}\left(\frac{2}{N_m\,(N_m-1)}\sum_{i,j\in m}A_{i,j} - \frac{1}{N_m N_n}\sum_{p\in m,q\in n}A_{p,q}\right)$$

All forms of SID values defined above are derived as a pair-wise summation of differences of within-subnetwork and between-subnetwork strengths. Thus, an increase in SID suggests increased segregation between subnetworks that are driven either by an increased within-subnetwork strength for the given subnetwork or a decreased between-subnetwork strength with regard to all other subnetworks. On the other hand, a decrease in SID implies an increase in integration, which is caused either by decreased within-subnetwork strength and/or an increased between-subnetwork strength.

The Bayley Scales of Infant Development, 3rd Ed (BSID-III) (Connolly et al. 2006), which have been used widely regarding outcome following perinatal brain injury (Miller et al. 2005), were performed by a developmental psychologist. This assessed motor, cognitive and language development.

Statistical Analysis

We separately compared between any pair of SI, NMI and HT groups using permutation tests with 1000 repetitions. The number of permutations commonly used in literature is up to 10 000. Due to the high computational cost of constructing structural covariance in our large network using the GLM that includes several covariates, however, a relatively smaller permutation number was selected as a reasonable compromise considering the time requirement and computational cost. Specifically, in each run of permutation, all patients were randomly assigned into the six subgroups. The number of patients within each group was same as six subgroups in real conditions. Structural covariance was then generated, and graph theoretical variables were computed using sulcal depth values from randomly assigned patients. For each time range and variable, the actual difference between the given two groups was placed in its corresponding permutation distribution to obtain the significance level (95%). Finally, the false discovery rate (FDR) of P-values from all variables and time ranges was controlled and adjusted using the previously described procedures (Benjamini and Hochberg 1995).

Results

Cortical Folding Trajectory in NMI and SI Preterm Neonates

Vertex-wise sulcal depth values were computed and mapped for 229 scans of NMI and SI preterm neonates at three developmental time frames as displayed in Figure 2 (Demographics found in Table 1). Sulcal depth values were also calculated in 40 HT newborns and were mapped in the last time frame of Figure 2. Mapping of three neurodevelopmental time frames of the third trimester demonstrated rapid sulcal deepening in NMI and SI groups in the early and middle time frames before plateauing by late stage of third trimester. However, the SI group exhibited significantly shallower sulci ($P = 0.01$; $t = 2.67$) compared with the NMI group in only the early time range, while no differences were found in the middle or late time periods (middle: $P = 0.12$, $t = 1.62$; late: $P = 0.69$, $t = 0.40$) due to SI group's faster growth rate. To account for repeated scans per subject and variance among sulcal depths, a mixed-effects nonlinear model with polynomial fitting was also modeled to sulcal depth changes along with age. This analysis produced similar trends to the initial analysis that accounted for three age groups (Supplementary Fig. 4).

Sulcation measurements of HT infants plotted at their neonatal scan (approx. 40th week) were found to be slightly higher than both NMI and SI preterm infants, although no significant differences were found ($P > 0.19$; $t < 1.31$ compared with NMI, and $P > 0.51$, $t < 0.65$ compared with SI). Sulcal depth values quantified for each group can be found in Supplementary Table 1. Further analysis of MRI strength (3 T vs. 1.5 T) demonstrated that different field strengths of MRIs did not affect sulcal depth values and cortical regional patterns (Supplementary Fig. 5).

Cortico-cortical Covariance of Sulcation and Differences Between NMI and SI Groups

Our analysis of sulcal depth correlations showed hyper-covariance—increased global covariance strength in the SI group compared with the NMI group. This difference was exhibited in the early stage of third trimester ($P = 0.002$; Fig. 3A; permutation test) in which lack of cortical folding was observed in Figure 2. However, such hyper-covariance was diminished in the later stages ($P > 0.11$) in which rapid sulcal deepening was

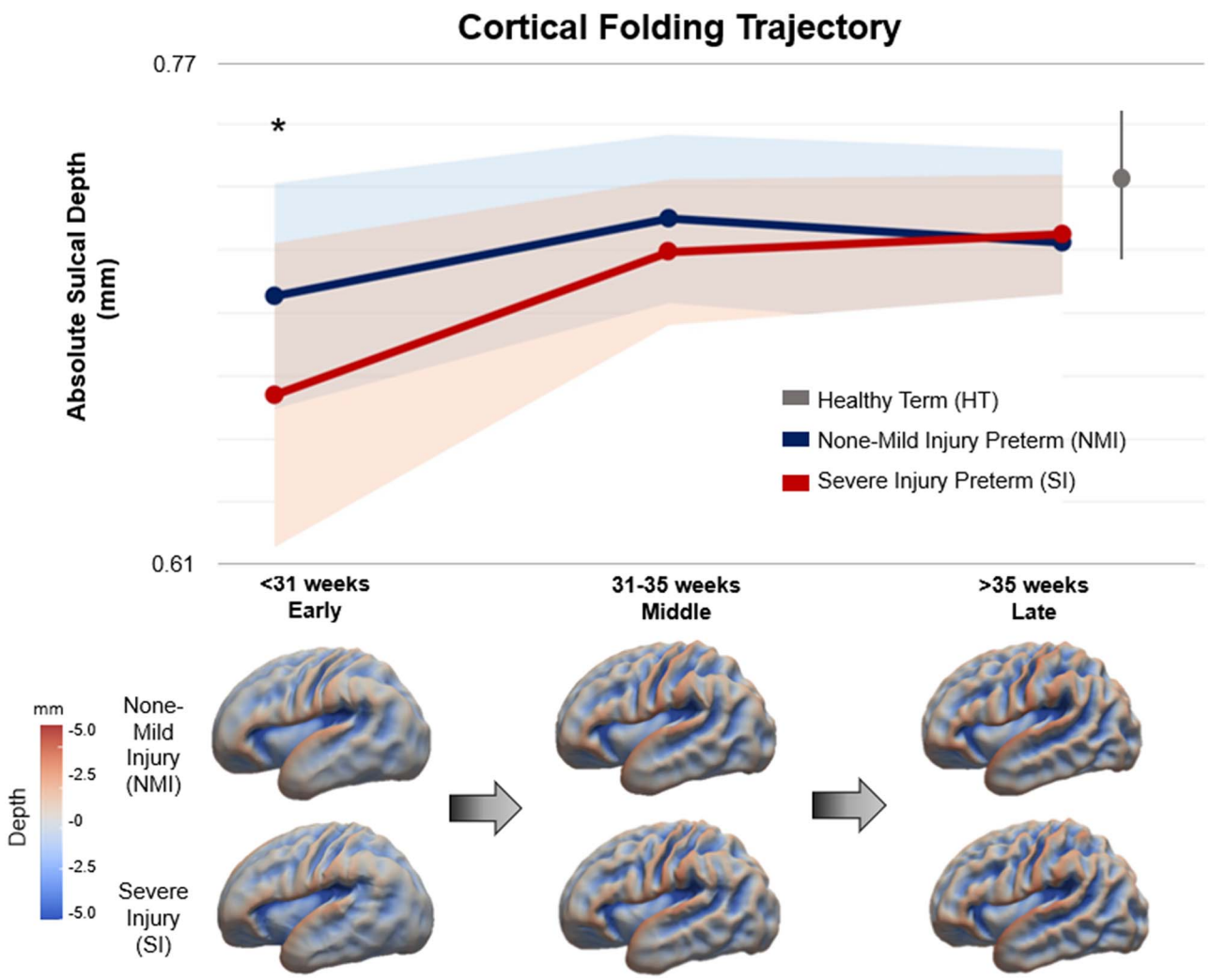

Figure 2. Cortical folding trajectory of NMI and SI preterm neonates. Both NMI and SI groups exhibit similar trends of rapid cortical folding expansion in the early and middle stages of the third trimester, thereafter, plateauing by the late stage. However, the SI group displays significantly shallower sulci in the early stage ($P = 0.01$; $t = 2.67$), while no differences are found in the middle or late time frames due to their faster growth. The average sulcation value of HT neonates is plotted at term (40th week of gestation). Sulcation values of HT neonates are higher than both NMI and SI preterm born neonates, although not significantly different. For NMI and SI preterm groups, circles represent their means and shaded bands represent their standard deviations. The standard deviation for HT infants is shown as the vertical gray line to the right of the graph.

exhibited in SI group, suggesting their *catching-up* process (Figs 2 and 3A). The developmental trajectory of covariance strength was inverted from that of sulcal depth expansion throughout preterm gestation.

Analyzing regional covariance strength between NMI and SI neonates, significant differences of correlation strength between the two groups were mapped on the cortical surface ($P < 0.05$; Fig. 3B; permutation test, corrected using FDR). Significant regional differences in covariance strength were the most widespread in the early stage, while decreasing substantially by the middle and late stages. After FDR correction, significant differences in the early stage were found in sulcal/gyral areas including bilateral (anterior) superior temporal, anterior cingulate, central and insular cortices, in the right angular and precuneus cortices, and in Broca's area of the left inferior frontal gyrus. Residual regional differences by the late stage, which was not captured by global connectivity measures, were still observed in the left posterior cingulate cortex ($P < 0.05$).

Structural covariance of HT neonates (at the 40th week) was also calculated and plotted. HT neonates exhibited slightly lower covariance strength compared with both preterm neonate groups, but this pattern was not significant ($P > 0.37$). No hyper-covariance in the SI group relative to the NMI group was found ($P > 0.26$). Covariance strength values quantified for each group can be found in Supplementary Table 2.

Network-Level Integration and Segregation of Corticocortical Covariance

Graph theory-based analyses were utilized to quantitatively compare topological properties of sulcation-based covariance networks among NMI and SI preterm as well as HT neonates. Compared with the NMI group, the SI group exhibited decreased network integration (Fig. 4A) in both the early and late time periods, characterized with decreased global efficiency

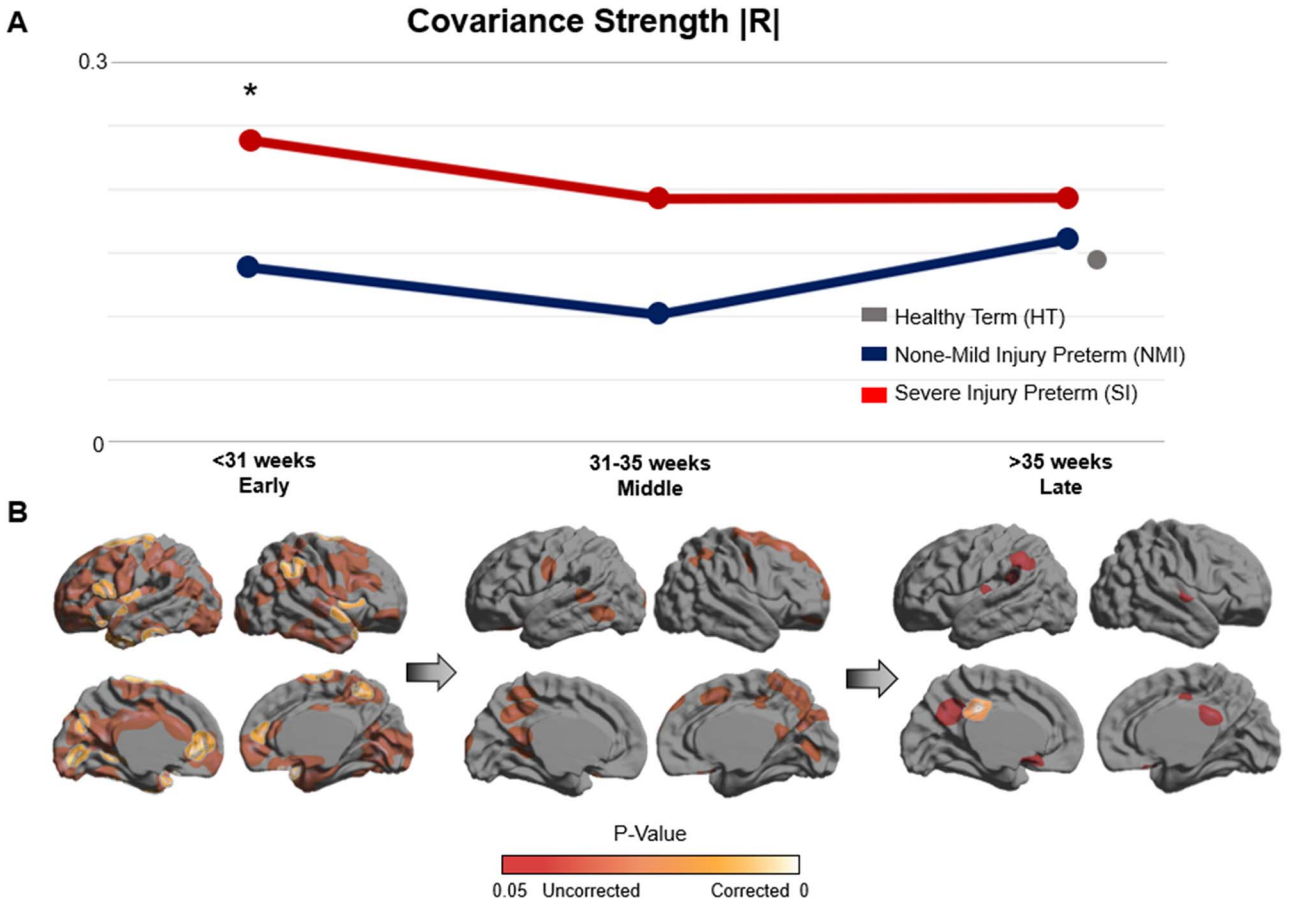

Figure 3. Network-level structural covariance of cortical sulcation. (*A*) The line graph depicts the developmental trajectory of global covariance strength |R| in NMI and SI preterm neonates. Inverted from trends exhibited in cortical folding, the SI group displays significantly increased covariance strength ($P = 0.002$; permutation test), suggesting maturational hyper-covariance in the early time frame. No significant differences between the NMI and SI groups are found in the middle or late time frames. Covariance strength of HT neonates is also plotted in gray and appears to lie within similar range as both NMI and SI preterm neonates. (*B*) Regions of significant differences between NMI and SI groups in terms of global covariance strength are mapped across all time points. The early stage exhibits the most widespread significant differences, while such differences gradually diminish throughout the middle and late stages. Residual differences of global covariance strength persist up until the late stage of the third trimester.

(early: $P = 0.01$, late: $P = 0.04$, permutation test) and increased characteristic path length (early: $P = 0.01$, late: $P = 0.049$). By contrast, the SI group exhibited increased network segregation (Fig. 4*B*), demonstrated with increased modularity (late: $P = 0.049$) and increased clustering coefficient (early: $P = 0.01$, late: $P = 0.02$).

In the last time frame, the HT group exhibited significantly greater measures of network integration compared with SI but no difference compared with NMI: global efficiency (HT vs. SI $P = 0.007$, HT vs. NMI $P = 0.3$) and characteristic path length (HT vs. SI $P = 0.007$, HT vs. NMI $P = 0.5$). On the other hand, the HT group exhibited no difference in network segregation compared with both SI and NMI groups: clustering coefficient (HT vs. SI $P = 0.3$, HT vs. NMI $P = 0.5$) and modularity (HT vs. SI $P = 0.4$, HT vs. NMI $P = 0.3$). Network analyses of HT neonates are shown in the Supplementary Section (Supplementary Table 3 and Supplementary Figs 1–3).

SI Preterm Neonates Exhibit Reduced Integration of Large-Scale Networks by the Late Period of the Third Trimester

For the late stage of the 3rd trimester in which the global topological properties of covariance networks were different between SI and NMI groups, *segregation integration difference* (SID) for all subnetworks and global SID were compared among SI and NMI preterm as well as HT neonates in the late time frame using permutation test (Table 4 and Fig. 5).

Results demonstrated significantly reduced global integration strength (Global SID) of large-scale networks in preterm neonates with SI compared with those of NMI and HT neonates (SI vs. NMI $P = 0.011$, SI vs. HT $P = 0.022$). Specifically, this reduced integration in SI was found in the dorsal attention, frontoparietal, and limbic networks (SI vs. NMI $P = 0.025$, $P = 0.025$, $P = 0.025$, SI vs. HT $P = 0.045$; illustrated in Table 6 and Fig. 5). In visual network, SI group additionally showed reduced integration compared with NMI preterm neonates ($P = 0.025$). No significant differences in integration strength were exhibited in ventral attention, auditory, salient, default mode, and sensory motor systems ($P > 0.5$).

Bayley Scales of Infant Development (Bayley-III) at 18 months including assessments of cognitive, language, and motor functions, were compared between SI and NMI neonates using a two-tailed *t*-test (Supplementary Table 6). Scores for HT neonates were unavailable and thus were not included in this analysis. SI neonates exhibited significantly lower scores in cognitive ($P = 0.006$) and motor ($P = 0.013$) assessments compared with NMI neonates. No significant difference was found in

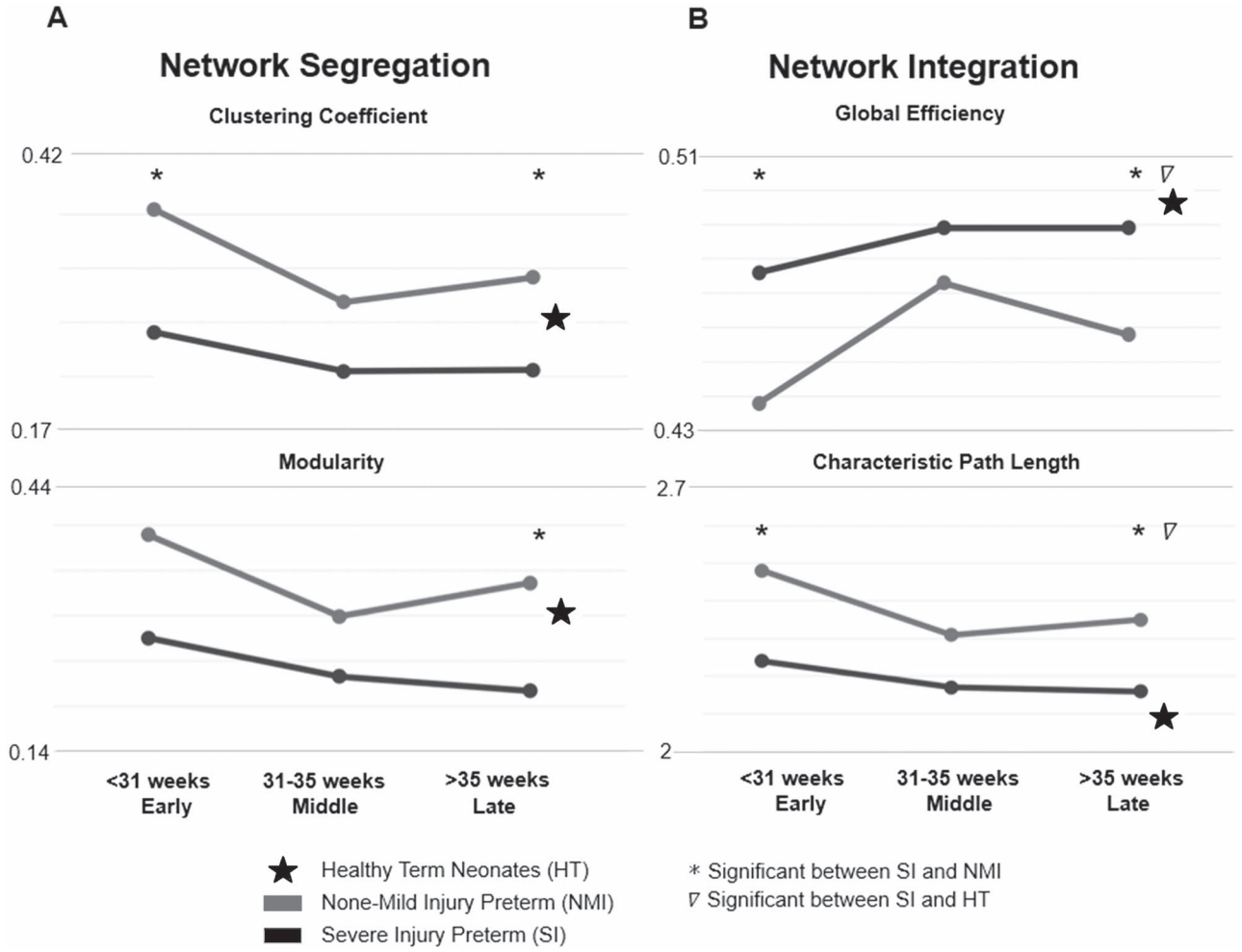

Figure 4. Graph theory analysis of sulcation-based covariance networks. (*A*) The SI group exhibits significantly increased levels of network segregation (increased clustering coefficient and increased modularity). While the clustering coefficient is significantly increased in both the first- and last-time frames, modularity was significantly increased in only the third time frame. (*B*) The SI group displays significantly decreased levels of network integration (lower global efficiency, higher characteristic path length). For all integration metrics, significant differences between NMI and SI groups are found in both the early and late time frames.

Table 4 Global and network SID network analysis

Network	Severe injury (SI)	None—mild injury (NMI)	HT
Global SID	3.285[a,b]	1.708	1.904
Frontoparietal	0.248[a,b]	0.134	0.137
Visual	0.348[a]	0.198	0.228
Dorsal attention	0.412[a,b]	0.218	0.180
Limbic	0.378[a,b]	0.221	0.260

[a]Significant between SI and NMI.
[b]Significant between SI and HT.

language scores. Additionally, no significant correlation was found between cortical folding and Bayley scores.

Discussion

We found that severe perinatal brain injures lead to reduced cortical folding in the earliest stage of the third trimester, although such abnormal cortical folding seemingly recovers to normal levels later. The time at which cortical folding abnormalities occur overlaps with the period at which hyper-covariance occurs, suggesting that the two events may be related. Essentially, the accelerated cortical folding observed following the presence of perinatal brain injury (Fig. 1) and the simultaneously found hyper-covariance (Fig. 2) possibly is an indicator of the presence of some mechanism of compensation, neuroplasticity, and recovery. Indeed, a temporal correlation between these events does not prove a direct causal association; however, this hypothesis may explain how the early brain develops after neurological insult. But despite this

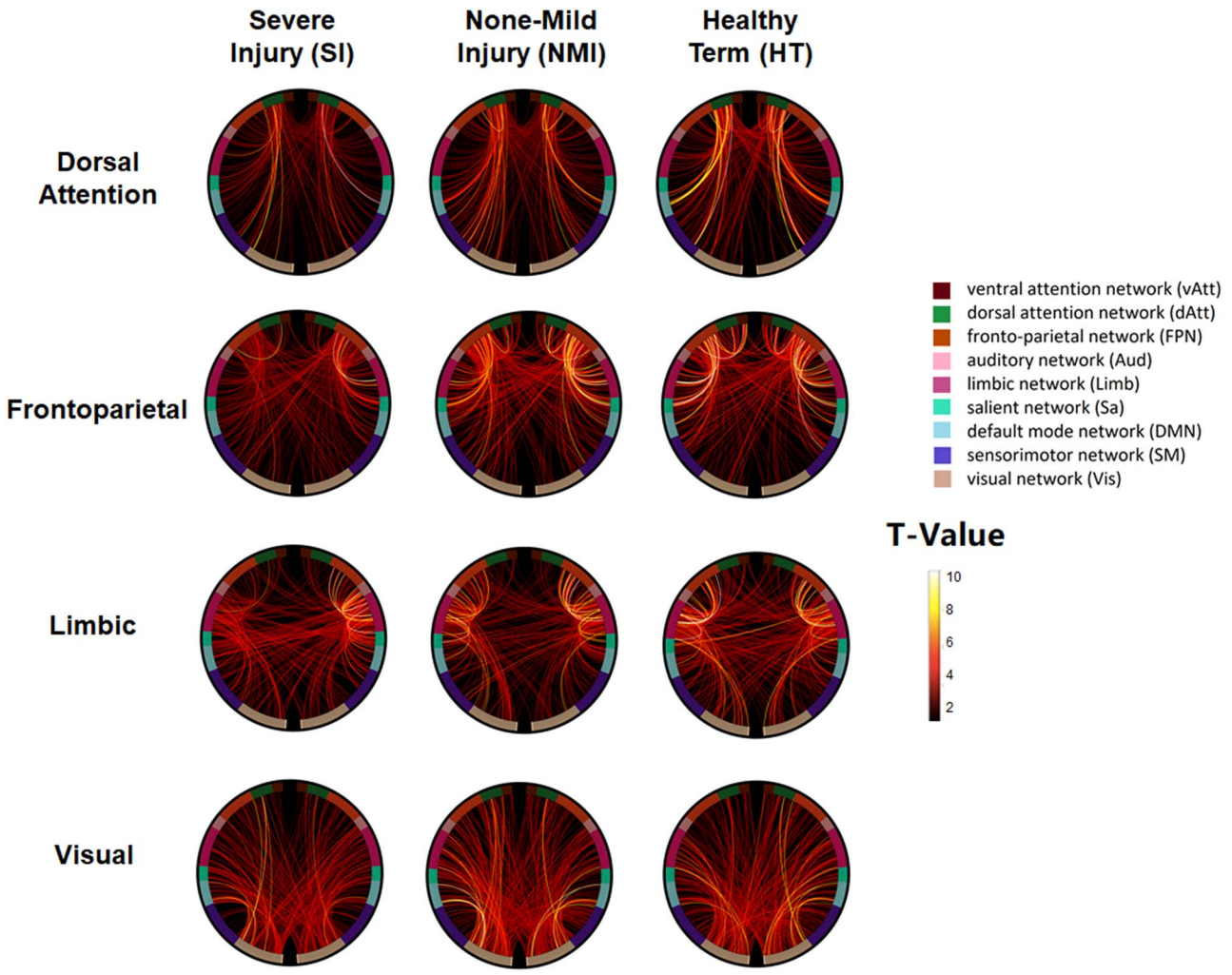

Figure 5. Reduced integration of large-scale networks in SI group relative to NMI group. The presence of a connection indicates that a significant correlation or degree of integration exists between any two large-scale networks which are labeled in the outer most edge of the connectogram. Each large-scale network is displayed as part of the circle of radially aligned elements. Connection strength and large-scale network integration are indicated through colored lines within the circular graphs that represent associations among analyzed large-scale resting state networks. The SI group exhibits significantly reduced connections and integrations in the following large-scale resting state networks: dorsal attention, frontoparietal, limbic, and visual. However, no significant differences in connection strength and integration are found in the following large-scale resting state networks: ventral attention, auditory, salient, default mode, and sensory motor systems. HT infants also exhibit significantly higher network integration metrics compared with SI preterm infants for all large-scale networks except for visual. More details can be seen in Table 4.

compensatory or recovery process, we also found residual aberrations of decreased network integration and increased segregation in SI brains at the late third trimester, implicating a suboptimal and inefficient topological organization. Additionally, SI brains exhibited reduced integration of large-scale networks, which may be associated with poor clinical outcome of higher cognitive function in premature neonates with severe perinatal injuries.

Hyper-covariance Associated with Compensation, Brain Plasticity, and Recovery of Cortical Folding

Both NMI and SI preterm neonates exhibited similar trends in cortical folding expansion, whereby sulcation rapidly increased in the early and middle stages before plateauing by the late stage of the third trimester. Cortical folding and covariance strength in the late stage of both SI and NMI preterm neonates appear to be similar to those exhibited in HT neonates. However, compared with the NMI group, the SI group exhibited significantly decreased sulcation in the early stage only. The sharper acceleration of cortical folding in their later stages may be indicative of compensation, brain plasticity, or recovery, whereby the injured brain may attempt to "catch up" with the trajectory of normal brain growth. Compensatory mechanisms of recovery have been noted in multiple studies that shed light on the preterm brain's ability to recover from prematurity-related or severe perinatal injuries by means of neural network plasticity (Inder and Volpe 2000; Scafidi et al. 2009; Harris et al. 2016).

Our investigation of sulcation-based structural covariance networks showed hyper-covariance in the SI group only in the early stage where reduced folding was observed. One possible explanation is that hyper-covariance may be a driver of the injured preterm brain's ability to compensate or recover from neurological insult. In other words, increased covariance may be a biomarker of the injured brain's respondence to neurological or white matter insult through the amplification of interregional

trophic signaling for plasticity, recovery, and reorganization of brain systems (McAlonan et al. 2005; Mitelman et al. 2005). Likewise, recovery may be induced by means of increased interaction between two regions that more effectively send trophic signals after severe neurological insult (Alexander-Bloch, Giedd, et al. 2013a). Analysis in nonhuman primates also demonstrated that lesions lead to new and abnormal cortical folding in distant but synaptically related cortical regions, suggesting that one neural population can affect another neural population of a distant cerebral structure (Rakic 1988). Considering this concept, one may speculate that hyper-covariance may underlie compensatory cortical folding of one cortical region when another is insulted during neurodevelopment. The perinatal injuries that we analyzed are all distant from the cortex (i.e., WM injury, VM, and IVH), suggesting that accelerated cortical expansion together with hyper-covariance is indeed plausible in the event of insult.

Of note, the underlying mechanism of hyper-covariance remains to be clarified, as there have been no previous studies investigating this phenomenon in the preterm cohort. However, such concept of hyperconnectivity has been explored in resting state functional networks of the adult brain in response to traumatic brain injury (TBI) (Hillary et al. 2011; Iraji et al. 2016). Indeed, it has been proposed that hyperconnectivity exhibited after TBI is a mechanism of the brain's plasticity and recovery process. Intriguingly, such hyperconnectivity leads to adverse cognitive outcomes in later years (Harris et al. 2016), which is similar to cognitive, behavioral, and language impairments that are commonly exhibited in preterm survivors born with perinatal brain injuries (Hamrick et al. 2004; Miller et al. 2005). Past studies have also shown that functional hyperconnectivity, as a result of neurological injury, is associated with disruptions of white matter integrity that connect cortical regions involved in cognition, suggesting that the adverse effects of hyperconnectivity are not only limited to brain function but also to its structure (Hillary and Grafman 2017).

Additionally, one may consider that hyper-covariance observed in the early time frame may be due to smoother brain topology. However, we would like to point out that a smoother brain or delayed brain maturation does not necessarily increase structural covariance. In studies where children with delayed brain maturation were analyzed (decreased in cortical thickness and gray matter volume), mixed decreased and increased local structural covariances were found (Nosarti et al. 2011; Bethlehem et al. 2017). Although this is not a direct analysis within our SI cohort, this data may support the notion that the observed hyper-covariance is not merely due to the initial "smoother" topography but rather to an underlying pathological process associated with neurological injury and recovery.

SI Preterm Neonates Exhibit Residual Aberrations of Covariance Network Topology

Compensatory development of cortical folding and covariance networks are notable examples of the neonatal brain's remarkable properties of plasticity and recovery. However, our study suggests that such recuperative processes may be incomplete or aberrant, considering our discovery of residual aberrations in graph theoretical network topology by the late third trimester.

Our findings demonstrated that the NMI preterm brain has a neurodevelopmental trend of gradually increasing measures of global integration and decreasing measures of segregation. This phenomenon is consistent with previous findings that prenatal and early postnatal brain development is characterized by a transition from local, proximity-based connectivity patterns to a more integrated topology imperative to higher-order cognitive functions (Fan et al. 2011; Khundrakpam et al. 2013; van den Heuvel et al. 2015).

Furthermore, in contrast to both NMI preterm and HT neonatal brains, the SI brain induces a significant reduction of network integration, which accounts for the capacity of a brain (or set of brain regions) to consolidate and communicate information. In other words, the SI brain exhibits disrupted efficiency in transferring information between and across remote regions. Past studies also suggest that neurodevelopmental disorders are associated with decreased efficiency and communication across regions of the brain (van den Heuvel and Sporns 2011). For instance, executive function disorders in preterm children were shown to be associated with widespread abnormalities, rather than focal lesions, of both white and gray matter (Boardman et al. 2010; Anderson et al. 2017). Such widespread abnormalities may be more likely to disrupt global integrated network topology associated with higher-order cognitive functions (Fischi-Gomez et al. 2016).

Our results also demonstrate that severe neurological injuries are associated with increased network segregation in terms of clustering coefficients and modularity, which are used to characterize the influence of functionally distinct brain networks on different cognitive behaviors (Watts and Strogatz 1998). Structural brain modules are known to become more segregated during development (Baum et al. 2017), indicating that a normal range of enhanced segregation strengthens regionally selective functional dependency. Abnormally increased network segregation in SI preterm brains may, therefore, reinforce excessive trophic influence on topologically constrained proximal regions rather than on remote regions. Such abnormally segregated networks are also known to lower resilience in persons exposed to a brain disorder or functional impairment (Schreiber et al. 2016).

Past studies confirm aberrations in the preterm brain connectome (Rubinov and Sporns 2010; Vertes and Bullmore 2015; Fischi-Gomez et al. 2016). We advanced these findings to new evidence that the SI group exhibits combined alterations of network integration and segregation in the early stage that persist into the last stage of the third trimester. Such residual aberrations in network topology in the SI group, despite a "catching-up" process, suggest disturbance in the normal balance between local specialization and global integration (Sporns et al. 2000; Brown et al. 2014).

Injured Preterm Neonates Exhibit Reduced Integration of Large-Scale Functional Networks

Given that abnormal topology of covariance networks was globally found in the SI preterm, we aimed to understand whether neurological injury also influences the integration of large-scale brain networks that involve different cortical regions in each modular network and are indicative of higher-order cognitive functions. These large-scale networks are an important area of study, given that most higher-order cognitive behaviors are not contingent upon an individual brain region in isolation but rather a group of networks integrating with each other (Cocchi et al. 2013; Sporns 2014; Bassett et al. 2015). Our results demonstrated that *severe brain injuries may lead to significantly reduced large-scale network integration compared with both NMI preterm and HT brains*. This residual disintegration of large-scale brain networks in SI preterm neonates may be associated with the manifestation of cognitive abnormalities in a proportion

of preterm survivors later in their school ages (Fischi-Gomez et al. 2015; Fischi-Gomez et al. 2016). Thus, a comprehensive understanding of network properties may provide more insight on potential neurodevelopmental deficits, which cannot be substantiated by analyzing cortical folding measure alone, given that we observe SI brains recover their cortical folding expansion to normal levels of development.

More specifically, SI preterm brains exhibited significantly reduced connectivity of the dorsal attention, frontoparietal, limbic, or visual systems with other functional networks. Reduced integration of the dorsal attention and frontoparietal networks may implicate the brain's lack of efficiency in executing higher cognitive function and attention-demanding tasks (Sturm et al. 1999; Spreng et al. 2013). Likewise, reduced integration of the frontoparietal network may suggest that the injured preterm brain is at risk of reduced ability to control behavior related to emotional processing, learning, and memory, as this network is tightly interconnected with both cortical and subcortical structures (amygdala, hippocampus, cingulate gyrus, and nucleus accumbens) (Barrett and Satpute 2013). Additionally, reduced integration in the limbic network may be associated with abnormal emotional behaviors (Drevets et al. 2008), while reduced integration in the visual network may be associated with visual problems that are often noted in preterm subjects born with brain injury (Fazzi et al. 2009; Hreinsdottir et al. 2013).

Injured Preterm Neonates Exhibit Poor Cognitive and Motor Outcome in Later Years

Previous studies have established an association between severe perinatal brain injuries and neurologic outcome of preterm neonates (Mercuri et al. 2003, 2004). Significantly lower scores in cognitive and neuromotor performance in SI neonates suggest that neurological injury transpiring at the third trimester of gestation is an important predictor of impaired brain functions in later years. However, no significant association was observed between cortical folding and Bayley score outcomes. This may be due to the notion that cortical folding was found to recover to normal levels in the SI cohort by the late stage of the third trimester, suggesting that this cortical maturational characteristic may minimally influence on the postnatal neurocognitive, language and motor development. Poor neurodevelopmental outcome in the SI group may be led by other aspects of brain maturation, such as myelination, white matter connectivity or cortical thickening.

Limitations and Future Directions

There are several limitations to consider in this study. Our study did not adopt a true longitudinal analytic method, in which we assigned each scan into the groups representing various time points of the third trimester of gestation. Despite availability of up to two postnatal scans acquired per baby, such categorization of scans in a cross-sectional manner may lead to confounds in our results. One issue may be related to the variability of postnatal age at scan, as the baseline scan would have been acquired right after birth whereas the follow-up scan would be taken after a longer period. We attempted to address such confounds by including each scan's subject birth age as a covariate, thereby correcting for possibly different folding rates between prenatal and postnatal growths.

The relationship of neonatal covariance networks with neurodevelopmental outcome in preterm survivors remains to be clarified in our study. Future studies aiming to run a longitudinal study of brain development from the preterm gestational period ideally to childhood or adolescent years would provide better understanding of how covariance network and connectivity aberrations contribute to any neurological deficit observed in future years.

Sulcation-based covariance networks only indirectly explain the anatomical connectivity patterns, as opposed to diffusion imaging of white matter tracts. More specifically, properties of the covariance network do not reflect the presence of physical connections of information flow across cortical regions as they are statistical structures, and therefore may somewhat deviate from the true essence of connectivity information. On the other hand, covariance network analyses have been favored in the investigation of trophic pathways of developing brains where morphological growth is vigorous (Mechelli et al. 2005; Alexander-Bloch, Raznahan, et al. 2013b). Structural covariance networks cannot be extrapolated to network parameters at the individual level, thus obstructing correlations with clinical scores of preterm infants. Given the presence of multiple longitudinal scans, a recent study built individual covariance networks that link to individual variability in cognition and disease severity (Khundrakpam et al. 2019). We are currently aiming to pursue this direction of analysis for individual covariance using our longitudinal cohorts.

Although our study analyzed the severity of neurological injury through a composite scoring system, we did not consider the influence of each individual injury separately (IVH, VM, WMI), which may impact the brain development through distinct pathological mechanisms as seen in previous studies (Kim, Gano, et al. 2016a; Smyser et al. 2019). Our study was not able to analyze each injury individually due to a relatively small sample size, confining us to analyze all severe neurological injury collectively within one cohort. However, considering that these injuries are similarly involved in lesions around the cerebral ventricles, we consider it rather likely that these injuries may have underlying common influences on resulting ectopic cortical folding as a whole, which is what was primarily examined through the global covariance metric. For instance, the radial unit hypothesis explains how cerebral expansion originates from the ependymal layer of the cerebral ventricle, which consists of proliferative radial glial cell units that prefigure cytoarchitectonic areas of the cortex (Rakic 1988). Abnormal migration of these radial glial cells can lead to alterations in cortical folding resulting in lissencephaly (smooth brain) or polymicrogyria (too many folds) (de Juan Romero et al. 2015). Essentially, PVL, VM, and IVH, albeit different in pathological etiologies, may have commonality in disrupting the proliferative process of radial glial cells and cortico-cortical connections associated with cortical folding. This is not to say that differences in pathological etiology and lesion location are not important to consider, as their underlying pathophysiology on cortical development are indeed different (Volpe 2009). However, specifically in the context of sulcation and its covariance, such different etiologies may not have as significant of differential effects compared with the severity of injury itself. Similar to our study, other studies showed the effects of different brain injuries on cerebellar growth (Tam et al. 2011) and neurodevelopmental outcome (Guo et al. 2017). To further validate the lack of influence by different pathological etiologies on our results, we demonstrated in another analysis that no significant differences in cortical folding or covariance outcome are observed among PVL, VM and IVH groups.

Additionally, there are additional perinatal risk factors such as birth weight, steroid treatment, neonatal intensive care factors (surgery, infection), cardiorespiratory conditions, injuries, or duration of prematurity (although most of our study samples were very preterm). Due to a range of perinatal factors, preterm infants are at risk for a wide range of intracranial complications. To consider various clinical confounds, each clinical characteristic listed in Table 1 was corresponded to each individual severe injury type: IVH, WMI, and VM (Supplementary Table 4). No significant difference was found between IVH and WMI groups for each clinical characteristic (VM was not analyzed due to small sample size), suggesting that our results may not have been obscured by clinical confounds.

Conclusion

We were able to characterize cortical folding and covariance network developmental trajectories among NMI and SI preterm as well as HT neonates. We showed that in-depth spatiotemporal pattering of cortical folding and network-level structural covariance provide valuable insight on how the preterm brain recovers from severe injuries in critical state and which brain structures and functional networks develop with residual damages. Our finding of residual brain abnormalities by the late third trimester in the SI cohort may provide new perspective on clinician's care for preterm infants with critical injuries. More importantly, our study identifies a specific time window, early and middle third trimesters, that plays a highly crucial role in understanding the processes of compensation and recovery. Identification of this critical time frame could play a crucial role in tailoring clinical courses of action that may be time sensitive in the early developmental stages.

Finally, our study provides an important analytic framework whereby clinicians may attain a better understanding of how the brain changes during the early developmental period may affect health and cognition in future adolescent years. The current findings implicate that the brain connectome and network properties may contribute as clinical biomarkers indicative of higher-order cognitive functions. As such, neurodevelopmental outcomes in these higher-order domains may be better predicted with "connectome-type" analyses that incorporate measures of network segregation and integration (Fischi-Gomez et al. 2016) as opposed to a single morphological metric. Ultimately, with increased clarity of structural morphology and network properties of the preterm brain, a more thorough and evidence-based clinical intervention may be applied as a necessary protocol to circumvent risks of severe injury and neurodevelopmental deficits associated with prematurity.

Supplementary Material

Supplementary material can be found at *Cerebral Cortex* online.

Funding

National Institutes of Health (grants P41EB015922, U54EB020406, K01HD091283, U19AG024904, U01NS086090, 003585-00001, P01NS082330, R01HD072074); BrightFocus Research Grant award (A2019052S). Baxter Foundation Faculty Fellowship Award (to H.K.).

Notes

Authors would like to thank the Developing Human Connectome Project (dHCP). Corresponding author's address: 2025 Zonal Ave, Los Angeles, CA, USA, 90033. *Conflict of Interest*: None declared.

Author Contributions

S.Y.K. designed analytic framework, analyzed data, performed statistics, drafted manuscript, and created figures and tables.

M.L. designed analytic framework, analyzed data, performed statistics, drafted manuscript, and created figures and tables.

S.J.H. advised the study design and edited manuscript.

A.W.T. provided funding and edited manuscript.

A.J.B. provided funding, acquired clinical data, added clinical interpretation, and edited manuscript.

D.X. provided funding, acquired imaging data, preprocessed images, and edited manuscript.

H.K. provided funding, processed images, designed analytic framework, supervised the study, and edited manuscript.

References

Ahmann PA, Lazzara A, Dykes FD, Brann AW Jr, Schwartz JF. 1980. Intraventricular hemorrhage in the high-risk preterm infant: incidence and outcome. *Ann Neurol*. 7:118–124.

Alexander-Bloch A, Giedd JN, Bullmore E. 2013a. Imaging structural co-variance between human brain regions. *Nat Rev Neurosci*. 14:322–336.

Alexander-Bloch A, Raznahan A, Bullmore E, Giedd J. 2013b. The convergence of maturational change and structural covariance in human cortical networks. *J Neurosci*. 33:2889–2899.

Anderson PJ, Treyvaud K, Neil JJ, Cheong JLY, Hunt RW, Thompson DK, Lee KJ, Doyle LW, Inder TE. 2017. Associations of newborn brain magnetic resonance imaging with long-term neurodevelopmental impairments in very preterm children. *J Pediatr*. 187:58–65 e51.

Barrett LF, Satpute AB. 2013. Large-scale brain networks in affective and social neuroscience: towards an integrative functional architecture of the brain. *Curr Opin Neurobiol*. 23:361–372.

Bassett DS, Bullmore ET. 2009. Human brain networks in health and disease. *Curr Opin Neurol*. 22:340–347.

Bassett DS, Yang M, Wymbs NF, Grafton ST. 2015. Learning-induced autonomy of sensorimotor systems. *Nat Neurosci*. 18:744–751.

Baum GL, Ciric R, Roalf DR, Betzel RF, Moore TM, Shinohara RT, Kahn AE, Vandekar SN, Rupert PE, Quarmley M *et al*. 2017. Modular segregation of structural brain networks supports the development of executive function in youth. *Curr Biol*. 27:1561–1572 e1568.

Benjamini Y, Hochberg Y. 1995. Controlling the false discovery rate: a practical and powerful approach to multiple testing. *J Royal Stat Soc*. 57:289–300.

Bethlehem RAI, Romero-Garcia R, Mak E, Bullmore ET, Baron-Cohen S. 2017. Structural covariance networks in children with autism or ADHD. *Cereb Cortex*. 27:4267–4276.

Boardman JP, Craven C, Valappil S, Counsell SJ, Dyet LE, Rueckert D, Aljabar P, Rutherford MA, Chew AT, Allsop JM *et al*. 2010. A common neonatal image phenotype predicts adverse

neurodevelopmental outcome in children born preterm. *Neuroimage*. 52:409–414.

Brown CJ, Miller SP, Booth BG, Andrews S, Chau V, Poskitt KJ, Hamarneh G. 2014. Structural network analysis of brain development in young preterm neonates. *Neuroimage*. 101:667–680.

Cachia A, Paillere-Martinot ML, Galinowski A, Januel D, de Beaurepaire R, Bellivier F, Artiges E, Andoh J, Bartres-Faz D, Duchesnay E *et al*. 2008. Cortical folding abnormalities in schizophrenia patients with resistant auditory hallucinations. *Neuroimage*. 39:927–935.

Chen H, Zhang T, Guo L, Li K, Yu X, Li L, Hu X, Han J, Hu X, Liu T. 2013. Coevolution of gyral folding and structural connection patterns in primate brains. *Cereb Cortex*. 23:1208–1217.

Chi JG, Dooling EC, Gilles FH. 1977. Gyral development of the human brain. *Ann Neurol*. 1:86–93.

Cocchi L, Zalesky A, Fornito A, Mattingley JB. 2013. Dynamic cooperation and competition between brain systems during cognitive control. *Trends Cogn Sci*. 17:493–501.

Connolly BH, Dalton L, Smith JB, Lamberth NG, McCay B, Murphy W. 2006. Concurrent validity of the Bayley scales of infant development II (BSID-II) motor scale and the Peabody developmental motor scale II (PDMS-2) in 12-month-old infants. *Pediatr Phys Ther*. 18:190–196.

de Juan Romero C, Bruder C, Tomasello U, Sanz-Anquela JM, Borrell V. 2015. Discrete domains of gene expression in germinal layers distinguish the development of gyrencephaly. *EMBO J*. 34:1859–1874.

Drevets WC, Price JL, Furey ML. 2008. Brain structural and functional abnormalities in mood disorders: implications for neurocircuitry models of depression. *Brain Struct Funct*. 213:93–118.

Dubois J, Benders M, Borradori-Tolsa C, Cachia A, Lazeyras F, Ha-Vinh Leuchter R, Sizonenko SV, Warfield SK, Mangin JF, Huppi PS. 2008. Primary cortical folding in the human newborn: an early marker of later functional development. *Brain*. 131:2028–2041.

Dumoulin CL, Rohling KW, Piel JE, Rossi CJ, Giaquinto RO, Watkins RD, Vigneron DB, Barkovich JA, Newton N. 2002. Magnetic resonance imaging compatible neonate incubator. *Concept Magn Reson*, 15:117–128.

Fan Y, Shi F, Smith JK, Lin W, Gilmore JH, Shen D. 2011. Brain anatomical networks in early human brain development. *Neuroimage*. 54:1862–1871.

Fazzi E, Bova S, Giovenzana A, Signorini S, Uggetti C, Bianchi P. 2009. Cognitive visual dysfunctions in preterm children with periventricular leukomalacia. *Dev Med Child Neurol*. 51:974–981.

Fischi-Gomez E, Munoz-Moreno E, Vasung L, Griffa A, Borradori-Tolsa C, Monnier M, Lazeyras F, Thiran JP, Huppi PS. 2016. Brain network characterization of high-risk preterm-born school-age children. *Neuroimage Clin*. 11:195–209.

Fischi-Gomez E, Vasung L, Meskaldji DE, Lazeyras F, Borradori-Tolsa C, Hagmann P, Barisnikov K, Thiran JP, Huppi PS. 2015. Structural brain connectivity in school-age preterm infants provides evidence for impaired networks relevant for higher order cognitive skills and social cognition. *Cereb Cortex*. 25:2793–2805.

Geva R, Schreiber J, Segal-Caspi L, Markus-Shiffman M. 2014. Neonatal brainstem dysfunction after preterm birth predicts behavioral inhibition. *J Child Psychol Psychiatry*. 55:802–810.

Goldman-Rakic P, Rakic P. 1984. Experimental modification of gyral patterns. In: Geschwind N, Galaburda AM, eds. *Cerebral dominance: the biological foundation*, Cambridge, MA: Harvard University Press. pp. 179–192.

Goldman-Rakic PS, Schwartz ML. 1982. Interdigitation of contralateral and ipsilateral columnar projections to frontal association cortex in primates. *Science*. 216:755–757.

Guo T, Duerden EG, Adams E, Chau V, Branson HM, Chakravarty MM, Poskitt KJ, Synnes A, Grunau RE, Miller SP. 2017. Quantitative assessment of white matter injury in preterm neonates: association with outcomes. *Neurology*. 88:614–622.

Hamrick SE, Miller SP, Leonard C, Glidden DV, Goldstein R, Ramaswamy V, Piecuch R, Ferriero DM. 2004. Trends in severe brain injury and neurodevelopmental outcome in premature newborn infants: the role of cystic periventricular leukomalacia. *J Pediatr*. 145:593–599.

Harris NG, Verley DR, Gutman BA, Thompson PM, Yeh HJ, Brown JA. 2016. Disconnection and hyper-connectivity underlie reorganization after TBI: a rodent functional connectomic analysis. *Exp Neurol*. 277:124–138.

Hillary FG, Grafman JH. 2017. Injured brains and adaptive networks: the benefits and costs of Hyperconnectivity. *Trends Cogn Sci*. 21:385–401.

Hillary FG, Slocomb J, Hills EC, Fitzpatrick NM, Medaglia JD, Wang J, Good DC, Wylie GR. 2011. Changes in resting connectivity during recovery from severe traumatic brain injury. *Int J Psychophysiol*. 82:115–123.

Hreinsdottir J, Ewald U, Strand Brodd K, Ornkloo H, von Hofsten C, Holmstrom G. 2013. Ophthalmological outcome and visuospatial ability in very preterm children measured at 2.5 years corrected age. *Acta Paediatr*. 102:1144–1149.

Imamura T, Ariga H, Kaneko M, Watanabe M, Shibukawa Y, Fukuda Y, Nagasawa K, Goto A, Fujiki T. 2013. Neurodevelopmental outcomes of children with periventricular leukomalacia. *Pediatr Neonatol*. 54:367–372.

Inder TE, Volpe JJ. 2000. Mechanisms of perinatal brain injury. *Semin Neonatol*. 5:3–16.

Iraji A, Chen H, Wiseman N, Welch RD, O'Neil BJ, Haacke EM, Liu T, Kou Z. 2016. Compensation through functional hyperconnectivity: a longitudinal connectome assessment of mild traumatic brain injury. *Neural Plast*. 2016: 4072402.

Khundrakpam BS, Lewis JD, Jeon S, Kostopoulos P, Itturia Medina Y, Chouinard-Decorte F, Evans AC. 2019. Exploring individual brain variability during development based on patterns of maturational coupling of cortical thickness: a longitudinal MRI study. *Cereb Cortex*. 29:178–188.

Khundrakpam BS, Reid A, Brauer J, Carbonell F, Lewis J, Ameis S, Karama S, Lee J, Chen Z, Das S *et al*. 2013. Developmental changes in organization of structural brain networks. *Cereb Cortex*. 23:2072–2085.

Kim H, Gano D, Ho ML, Guo XM, Unzueta A, Hess C, Ferriero DM, Xu D, Barkovich AJ. 2016a. Hindbrain regional growth in preterm newborns and its impairment in relation to brain injury. *Hum Brain Mapp*. 37:678–688.

Kim H, Lepage C, Maheshwary R, Jeon S, Evans AC, Hess CP, Barkovich AJ, Xu D. 2016b. NEOCIVET: towards accurate morphometry of neonatal gyrification and clinical applications in preterm newborns. *Neuroimage*. 138:28–42.

Kliegman RM, Hack M, Jones P, Fanaroff AA. 1982. Epidemiologic study of necrotizing enterocolitis among low-birthweight infants. Absence of identifiable risk factors. *J Pediatr*. 100:440–444.

Kodric J, Sustersic B, Paro-Panjan D. 2014. Relationship between neurological assessments of preterm infants in the first 2

years and cognitive outcome at school age. *Pediatr Neurol*. 51:681–687.

Lefevre J, Germanaud D, Dubois J, Rousseau F, de Macedo Santos I, Angleys H, Mangin JF, Huppi PS, Girard N, De Guio F. 2016. Are developmental trajectories of cortical folding comparable between cross-sectional datasets of fetuses and preterm Newborns? *Cereb Cortex*. 26:3023–3035.

Lerch JP, Worsley K, Shaw WP, Greenstein DK, Lenroot RK, Giedd J, Evans AC. 2006. Mapping anatomical correlations across cerebral cortex (MACACC) using cortical thickness from MRI. *Neuroimage*. 31:993–1003.

Levitt P, Rakic P, Goldman-Rakic P. 1984. Region-specific distribution of catecholamine afferents in primate cerebral cortex: a fluorescence histochemical analysis. *J Comp Neurol*. 227:23–36.

Maggi EF, Magalhaes LC, Campos AF, Bouzada MC. 2014. Preterm children have unfavorable motor, cognitive, and functional performance when compared to term children of preschool age. *J Pediatr (Rio J)*. 90:377–383.

McAlonan GM, Cheung V, Cheung C, Suckling J, Lam GY, Tai KS, Yip L, Murphy DG, Chua SE. 2005. Mapping the brain in autism. A voxel-based MRI study of volumetric differences and intercorrelations in autism. *Brain*. 128:268–276.

Mechelli A, Friston KJ, Frackowiak RS, Price CJ. 2005. Structural covariance in the human cortex. *J Neurosci*. 25:8303–8310.

Mehlhorn AJ, Morin CE, Wong-You-Cheong JJ, Contag SA. 2017. Mild fetal cerebral ventriculomegaly: prevalence, characteristics, and utility of ancillary testing in cases presenting to a tertiary referral center. *Prenat Diagn*. 37:647–657.

Mercuri E, Anker S, Guzzetta A, Barnett AL, Haataja L, Rutherford M, Cowan F, Dubowitz L, Braddick O, Atkinson J. 2004. Visual function at school age in children with neonatal encephalopathy and low Apgar scores. *Arch Dis Child Fetal Neonatal Ed*. 89:F258–F262.

Mercuri E, Guzzetta A, Laroche S, Ricci D, vanhaastert I, Simpson A, Luciano R, Bleakley C, Frisone MF, Haataja L *et al*. 2003. Neurologic examination of preterm infants at term age: comparison with term infants. *J Pediatr*. 142:647–655.

Miller SP, Cozzio CC, Goldstein RB, Ferriero DM, Partridge JC, Vigneron DB, Barkovich AJ. 2003. Comparing the diagnosis of white matter injury in premature newborns with serial MR imaging and transfontanel ultrasonography findings. *Am J Neuroradiol*. 24:1661–1669.

Miller SP, Ferriero DM, Leonard C, Piecuch R, Glidden DV, Partridge JC, Perez M, Mukherjee P, Vigneron DB, Barkovich AJ. 2005. Early brain injury in premature newborns detected with magnetic resonance imaging is associated with adverse early neurodevelopmental outcome. *J Pediatr*. 147:609–616.

Mitelman SA, Buchsbaum MS, Brickman AM, Shihabuddin L. 2005. Cortical intercorrelations of frontal area volumes in schizophrenia. *Neuroimage*. 27:753–770.

Nordahl CW, Dierker D, Mostafavi I, Schumann CM, Rivera SM, Amaral DG, Van Essen DC. 2007. Cortical folding abnormalities in autism revealed by surface-based morphometry. *J Neurosci*. 27:11725–11735.

Nosarti C, Mechelli A, Herrera A, Walshe M, Shergill SS, Murray RM, Rifkin L, Allin MP. 2011. Structural covariance in the cortex of very preterm adolescents: a voxel-based morphometry study. *Hum Brain Mapp*. 32:1615–1625.

Papile LA, Burstein J, Burstein R, Koffler H. 1978. Incidence and evolution of subependymal and intraventricular hemorrhage: a study of infants with birth weights less than 1500 gm. *J Pediatr*. 92:529–534.

Perlman JM, Risser R, Broyles RS. 1996. Bilateral cystic periventricular leukomalacia in the premature infant: associated risk factors. *Pediatrics*. 97:822–827.

Perlman JM, Rollins N. 2000. Surveillance protocol for the detection of intracranial abnormalities in premature neonates. *Arch Pediatr Adolesc Med*. 154:822–826.

Power JD, Cohen AL, Nelson SM, Wig GS, Barnes KA, Church JA, Vogel AC, Laumann TO, Miezin FM, Schlaggar BL *et al*. 2011. Functional network organization of the human brain. *Neuron*. 72:665–678.

Rakic P. 1988. Specification of cerebral cortical areas. *Science*. 241:170–176.

Raznahan A, Lerch JP, Lee N, Greenstein D, Wallace GL, Stockman M, Clasen L, Shaw PW, Giedd JN. 2011. Patterns of coordinated anatomical change in human cortical development: a longitudinal neuroimaging study of maturational coupling. *Neuron*. 72:873–884.

Ronan L, Fletcher PC. 2015. From genes to folds: a review of cortical gyrification theory. *Brain Struct Funct*. 220: 2475–2483.

Rubinov M, Sporns O. 2010. Complex network measures of brain connectivity: uses and interpretations. *Neuroimage*. 52:1059–1069.

Scafidi J, Fagel DM, Ment LR, Vaccarino FM. 2009. Modeling premature brain injury and recovery. *Int J Dev Neurosci*. 27:863–871.

Schreiber S, Vogel J, Schwimmer HD, Marks SM, Schreiber F, Jagust W. 2016. Impact of lifestyle dimensions on brain pathology and cognition. *Neurobiol Aging*. 40: 164–172.

Sharda M, Khundrakpam BS, Evans AC, Singh NC. 2016. Disruption of structural covariance networks for language in autism is modulated by verbal ability. *Brain Struct Funct*. 221:1017–1032.

Smyser CD, Wheelock MD, Limbrick DD Jr, Neil JJ. 2019. Neonatal brain injury and aberrant connectivity. *Neuroimage*. 185:609–623.

Sporns O. 2014. Contributions and challenges for network models in cognitive neuroscience. *Nat Neurosci*. 17:652–660.

Sporns O, Tononi G, Edelman GM. 2000. Theoretical neuroanatomy: relating anatomical and functional connectivity in graphs and cortical connection matrices. *Cereb Cortex*. 10:127–141.

Spreng RN, Sepulcre J, Turner GR, Stevens WD, Schacter DL. 2013. Intrinsic architecture underlying the relations among the default, dorsal attention, and frontoparietal control networks of the human brain. *J Cogn Neurosci*. 25:74–86.

Sturm W, de Simone A, Krause BJ, Specht K, Hesselmann V, Radermacher I, Herzog H, Tellmann L, Muller-Gartner HW, Willmes K. 1999. Functional anatomy of intrinsic alertness: evidence for a fronto-parietal-thalamic-brainstem network in the right hemisphere. *Neuropsychologia*. 37: 797–805.

Tam EW, Miller SP, Studholme C, Chau V, Glidden D, Poskitt KJ, Ferriero DM, Barkovich AJ. 2011. Differential effects of intraventricular hemorrhage and white matter injury on preterm cerebellar growth. *J Pediatr*. 158:366–371.

van den Heuvel MP, Kersbergen KJ, de Reus MA, Keunen K, Kahn RS, Groenendaal F, de Vries LS, Benders MJ. 2015. The neonatal connectome during preterm brain development. *Cereb Cortex*. 25:3000–3013.

van den Heuvel MP, Sporns O. 2011. Rich-club organization of the human connectome. *J Neurosci*. 31:15775–15786.

Van Essen DC. 1997. A tension-based theory of morphogenesis and compact wiring in the central nervous system. *Nature*. 385:313–318.

Van Essen DC, Dierker D, Snyder AZ, Raichle ME, Reiss AL, Korenberg J. 2006. Symmetry of cortical folding abnormalities in Williams syndrome revealed by surface-based analyses. *J Neurosci*. 26:5470–5483.

Vertes PE, Bullmore ET. 2015. Annual research review: growth connectomics—the organization and reorganization of brain networks during normal and abnormal development. *J Child Psychol Psychiatry*. 56:299–320.

Volpe JJ. 1981. Neurology of the newborn. *Major Probl Clin Pediatr*. 22:1–648.

Volpe JJ. 1997. Brain injury in the premature infant—from pathogenesis to prevention. *Brain Dev*. 19:519–534.

Volpe JJ. 2009. Brain injury in premature infants: a complex amalgam of destructive and developmental disturbances. *Lancet Neurol*. 8:110–124.

Watts DJ, Strogatz SH. 1998. Collective dynamics of 'small-world' networks. *Nature*. 393:440–442.

Welker WI, Campos GB. 1963. Physiological significance of sulci in somatic sensory cerebral cortex in mammals of the family procyonidae. *J Comp Neurol*. 120:19–36.

White T, Su S, Schmidt M, Kao CY, Sapiro G. 2010. The development of gyrification in childhood and adolescence. *Brain Cogn*. 72:36–45.

Woodward LJ, Anderson PJ, Austin NC, Howard K, Inder TE. 2006. Neonatal MRI to predict neurodevelopmental outcomes in preterm infants. *N Engl J Med*. 355: 685–694.

Zilles K, Armstrong E, Schleicher A, Kretschmann HJ. 1988. The human pattern of gyrification in the cerebral cortex. *Anat Embryol*. 179:173–179.

Zilles K, Palomero-Gallagher N, Amunts K. 2013. Development of cortical folding during evolution and ontogeny. *Trends Neurosci*. 36:275–284.